Journal of Computational Physics **181,** 526–544 (2002)
doi:10.1006/jcph.2002.7140

A Moving Mesh Method for the Solution of the One-Dimensional Phase-Field Equations

J. A. Mackenzie and M. L. Robertson

Department of Mathematics, University of Strathclyde, Livingstone Tower, 26 Richmond Street, Glasgow, G1 1XH, Scotland
E-mail: jam@maths.strath.ac.uk, ta.mrob@maths.strath.ac.uk

Received September 27, 2001; revised May 23, 2002

A moving mesh method is developed for the numerical solution of one-dimensional phase-change problems modelled by the phase-field equations. The computational mesh is obtained by equidistribution of a monitor function tailored for the functional variation of the phase field in the interfacial region. Existence and uniqueness of the discretised equations using a moving mesh are also established. Numerical results are given for classical and modified Stefan test problems. The numerical algorithm is relatively simple and is shown to be far more efficient than fixed grid methods. © 2002 Elsevier Science (USA)

Key Words: phase change; phase field; equidistribution; moving meshes; adaptive method.

1. INTRODUCTION

There has been much recent interest in the modelling of solidification processes. The main challenge is to incorporate events on the smallest microstructural scales to the larger macroscopic scales. Classical Stefan models do not take account of important physical properties such as undercooling and surface tension. These effects are normally incorporated within modified Stefan models (see [14] and Section 2.1). The numerical simulation of the modified model requires the estimation of the curvature of the interface between the solid and the liquid phases. This is often a difficult task, especially in three dimensions or when phase fronts merge.

Phase-field (PF) models avoid the need to explicitly track the moving interface. This is done by introducing an auxiliary continuous order parameter p, which takes on constant values in the solid and liquid phases and has a rapid transition in the vicinity of the solidification front. While PF models have been successful in demonstrating qualitative behaviour such as dendritic growth [24], a more quantitative agreement with sharp interface models depends on the interfacial thickness being small [33]. As the phase field is almost constant

0021-9991/02 $35.00

away from the front it is clear that efficient numerical procedures to solve the PF equations should incorporate some form of mesh adaptation [26, 29, 31].

There has been a considerable development of moving mesh methods to solve partial differential equations (PDEs) with steep solution fronts. These include flame propagation problems, the resolution of boundary and interior layers, and travelling wave solutions of nonlinear reaction–diffusion equations. The general idea behind these methods is to combine an auxiliary equation describing the evolution of the mesh with a discretisation of the physical PDE in a moving reference frame. For one-dimensional problems a useful approach to construct the mesh equation is the concept of equidistribution, where some function (often referred to as a monitor function) is distributed uniformly over the domain [15]. Such a mesh is said to satisfy an equidistribution principle (EP). The monitor function should be related to the local difficulty in solving the given PDE. Most of the practical applications of these algorithms require that the EP be regularised in time, the monitor function be smoothed in space, and the moving mesh equation be discretised [16, 20]. The combined effect of all of these approximations is not well understood although some analysis of spatial smoothing has been carried out by Huang and Russell [21].

Recently, Mackenzie and Robertson [25] have developed a simple moving mesh startegy for interface propagation problems that avoids some of the approximations given above. This is achieved using an analytically integrable monitor function which automatically gives rise to a smooth mesh. The algorithm is relatively simple and has been shown to work well when applied to a regularised enthalpy formulation of classical Stefan problems. A related approach has also been used by Farrell and Drury [19] to construct moving mesh methods for nonlinear hyperbolic problems. The purpose of this paper is to consider the application of the moving mesh method of Mackenzie and Robertson to solve the one-dimensional PF equations. Based on an asymptotic expansion of the phase variable in the interface region we propose a monitor function which leads to a nonuniform mesh that automatically scales with the interface thickness. Furthermore, we show that the system of nonlinear algebraic equations arising from the discretisation has a unique solution.

An outline of the rest of this paper is as follows: In the next section we describe the modified Stefan and phase-field models. In Section 3 we present the moving grid algorithm along with the monitor function we propose for these problems. The iterative algorithm used to solve the mesh and physical PDEs is given in Section 4. Finally, in Section 5 we apply the moving mesh method to test cases involving a classical Stefan problem, a modified Stefan example with undercooling, and the stability of a solid sphere within its melt.

2. MODEL EQUATIONS

2.1. *Modified Stefan Model*

The modified Stefan model describes a heat conduction problem and the evolution of a sharp interface $\Gamma(t)$ within a region $\Omega \subset \mathbb{R}^n$. The objective is to find a temperature field $u(\boldsymbol{x}, t)$ and a curve $\Gamma(t) \subset \Omega$ that solves the nondimensionalised equations

$$\frac{\partial u}{\partial t} = K\nabla^2 u, \qquad \boldsymbol{x} \in \Omega\backslash\Gamma(t), \tag{2.1a}$$

$$Lv = -K[\nabla u]^+_-, \qquad \boldsymbol{x} \in \Gamma(t), \tag{2.1b}$$

$$u = -\frac{\sigma}{\Delta s}(\kappa + \alpha v), \quad \boldsymbol{x} \in \Gamma(t). \tag{2.1c}$$

Equations (2.1a) and (2.1b) describe the diffusion of heat within the domain and the release of latent heat across the phase-change interface. Here L is the latent heat per unit mass, K is the thermal diffusivity, v is the normal velocity of the interface, and $[\nabla u]_-^+$ is the jump in the normal component of the temperature gradient at the interface. Surface tension and undercooling effects are modelled by the extended Gibbs–Thompson relation (2.1c). The parameter σ is the surface tension, α denotes a kinetic undercooling coefficient, Δs is the entropy difference between the two phases, and κ is the sum of the principal curvatures at a point of the interface. The classical Stefan model is obtained from (2.1) by setting $\sigma = 0$. Numerical approaches for solving (2.1) require some form of front tracking to determine the curvature on the interface. An alternative is to use a so-called diffuse interface model that implicitly defines the position of the interface.

2.2. *Phase-Field Model*

The PF equations are derived using the idea of a phase order parameter p and Landau–Ginzburg theory. A free energy functional F is constructed in terms of the phase order parameter and other thermodynamic variables. For example,

$$F(p, u) = \int_\Omega \left[\frac{1}{2}\xi^2 (\nabla p)^2 + f(p, u) \right] d\boldsymbol{x}, \tag{2.2}$$

where ξ is a length scale and $f(p, u)$ is a free energy density. Various choices of the precise choice of f have been suggested, the most studied of which is the Caginalp potential [10]

$$f(p, u) = \frac{1}{8a}(p^2 - 1)^2 - 2up. \tag{2.3}$$

This density consists of a double-well potential with a depth measured by a parameter a and a term coupling p and u. The energy density has a lower free energy associated with the value $p = 1$, which corresponds to the pure liquid phase, and $p = -1$, which corresponds to the solid phase (see Fig. 1). The interfacial region corresponds to transitional states where

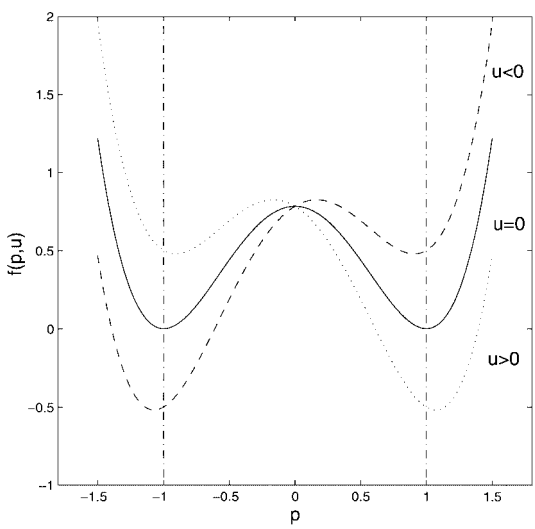

FIG. 1. Caginalp free energy density.

$-1 < p < 1$. The parameter a has to be small enough such that

$$\frac{\partial f}{\partial p} = \frac{1}{2a}(p^3 - p) - 2u = 0$$

has three distinct roots near $p = 0, \pm 1$. The parameters ξ and a are length scales related to the macroscopic physics. In particular, the surface tension σ and the interfacial thickness ε are related by

$$\sigma = \frac{2}{3}\varepsilon a^{-1} = \frac{2}{3}\xi a^{-1/2} \quad \text{and} \quad \varepsilon = \xi a^{1/2}. \tag{2.4}$$

A kinetic equation for the phase field is obtained by requiring that F monotonically decreases in time. The simplest choice of this requirement leads to the PF equation

$$\alpha\xi^2 \frac{\partial p}{\partial t} = -\frac{\delta F}{\delta p}, \tag{2.5a}$$

where $\alpha\xi^2$ is a relaxation time. The phase equation is conjoined with the heat equation, modified to take into account the liberation of latent heat by the inclusion of an appropriate source term:

$$\frac{\partial u}{\partial t} + \frac{L}{2}\frac{\partial p}{\partial t} = K\Delta u. \tag{2.5b}$$

Note that it is not clear whether the solution of (2.5) will result in F monotonically decreasing in time, as Eq. (2.5b) is not derived from basic thermodynamic principles. However, Penrose and Fife [28] have shown that the PF equations with the Caginalp free energy density can be derived in a thermodynamically consistent manner. Other thermodynamically consistent PF models have also been proposed [32]. However, it is not the purpose here to evaluate and compare the performance of the various models but to develop moving mesh methods as an efficient numerical solution procedure. Therefore, in the rest of this paper we will only consider the Caginalp free energy density, although the numerical approach can be applied to other formulations.

3. AN ADAPTIVE MOVING MESH METHOD

The aim of the phase-field model described here is to spread the phase change interface over a thin but finite region. The success of any numerical solution of the PF equations (2.5) requires that the interfacial region is well resolved. The computational mesh does not need to be as fine away from the interface where p and u are smooth.These demands clearly suggest than an efficient numerical method should involve some form of mesh adaptivity. For simplicity, we will concentrate on the one-dimensional PF equations and the use of moving mesh techniques.

Equations (2.5) are first recast in terms of the independent variables η and t, where η is defined by a one-to-one coordinate transformation of the form

$$x \equiv x(\eta, t), \quad \eta \in \Omega_c, \quad t \in (0, T], \tag{3.1}$$

from computational space $\Omega_c \times (0, T]$ to physical space $\Omega_p \times (0, T]$. Without loss of generality we will assume in this section that $\Omega_c = (0, 1)$. At time t, the map (3.1) defines a

set of nodes in Ω_p that corresponds to a uniform mesh on Ω_c. This uniform mesh is given by

$$\eta_j = j/N, \quad j = 0, 1, \ldots, N, \tag{3.2}$$

and the related grid on Ω_p is

$$\Delta_N := \{0 = x_0(t) < x_1(t) < \cdots < x_N(t) = 1\}, \tag{3.3}$$

where

$$x_j(t) = x(\eta_j, t), \quad j = 0, 1, \ldots, N. \tag{3.4}$$

The coordinate mapping that leads to the mesh adaptation is assumed to equidistribute a monitor function $M(x)$, which is the subject of Section 3.2.

It is convenient to express the time derivatives appearing in (2.5) in Lagrangian form and we therefore write the equations as

$$\dot{u} - \dot{x}\frac{\partial u}{\partial x} + \frac{L}{2}\left(\dot{p} - \dot{x}\frac{\partial p}{\partial x}\right) = K\frac{\partial^2 u}{\partial x^2}, \tag{3.5}$$

$$\alpha\xi^2\left(\dot{p} - \dot{x}\frac{\partial p}{\partial x}\right) = \xi^2\frac{\partial^2 p}{\partial x^2} - \frac{1}{2a}(p^3 - p) + 2u, \tag{3.6}$$

where $\dot{u}$, $\dot{p}$, and $\dot{x}$ denote derivatives with respect to t in which η is held constant.

In a moving mesh method a mesh generation equation, based on equidistribution of a monitor function, is combined with (3.5) and (3.6) to give a system of equations that determines $u(x(\eta, t), t)$, $p(x(\eta, t), t)$, and $x(\eta, t)$. To describe the discretisation we first introduce some notation. Let $h_j^n = x_j^n - x_{j-1}^n$ and $\Delta t^n = t^n - t^{n-1}$. We will also denote

$$\boldsymbol{u}_\Delta^n = \left(u_0^n, u_1^n, \ldots, u_N^n\right)^T, \quad \boldsymbol{p}_\Delta^n = \left(p_0^n, p_1^n, \ldots, p_N^n\right)^T,$$

where u_j^n and p_j^n are approximations of $u(x_j^n, t^n)$ and $p(x_j^n, t^n)$, respectively. We consider the following semi-implicit discretisations of (3.5) and (3.6):

$$\begin{aligned}
&\frac{u_j^{n+1} - u_j^n}{\Delta t^{n+1}} + \frac{L}{2}\frac{p_j^{n+1} - p_j^n}{\Delta t^{n+1}} - \frac{x_j^{n+1} - x_j^n}{\Delta t^{n+1}}\left(\frac{u_{j+1}^n - u_{j-1}^n}{h_{j+1}^n - h_j^n} + \frac{L}{2}\frac{p_{j+1}^n - p_{j-1}^n}{h_{j+1}^n + h_j^n}\right) \\
&\quad = \frac{2K}{h_{j+1}^{n+1} + h_j^{n+1}}\left(\frac{u_{j+1}^{n+1} - u_j^{n+1}}{h_{j+1}^{n+1}} - \frac{u_j^{n+1} - u_{j-1}^{n+1}}{h_j^{n+1}}\right),
\end{aligned} \tag{3.7}$$

$$\begin{aligned}
&\alpha\xi^2\left(\frac{p_{j+1}^{n+1} - p_j^n}{\Delta t^{n+1}} - \frac{x_j^{n+1} - x_j^n}{\Delta t^{n+1}}\frac{p_{j+1}^n - p_{j-1}^n}{h_{j+1}^n + h_j^n}\right) \\
&\quad = \frac{2\xi^2}{h_{j+1}^{n+1} + h_j^{n+1}}\left(\frac{p_{j+1}^{n+1} - p_j^{n+1}}{h_{j+1}^{n+1}} - \frac{p_j^{n+1} - p_{j-1}^{n+1}}{h_j^{n+1}}\right) - \frac{1}{2a}\left[\left(p_j^{n+1}\right)^3 - p_j^{n+1}\right] + 2u_j^n.
\end{aligned} \tag{3.8}$$

Note that the convection-like terms introduced by the movement of the mesh and the temperature term in (3.6) are treated explicitly, whereas all other terms are treated implicitly.

This has two important effects. First, it allows the equations to be solved in succession. That is, given an approximation $\{\boldsymbol{u}_\Delta^n, \boldsymbol{p}_\Delta^n\}$ we first solve (3.8) for $\boldsymbol{p}_\Delta^{n+1}$. We will show under a suitable condition on the time step that a unique solution exists. Thereafter, we solve (3.7) for $\boldsymbol{u}_\Delta^{n+1}$ and once again we will show that this can always be done uniquely.

3.1. *Iterative Solution of the Nonlinear System of Equations*

The calculation of $\boldsymbol{p}_\Delta^{n+1}$ requires the solution of (3.8), which, after multiplying through by Δt^{n+1}, can be written in the form

$$G\left(\boldsymbol{p}_\Delta^{n+1}\right) = A\boldsymbol{p}_\Delta^{n+1} + \phi\left(\boldsymbol{p}_\Delta^{n+1}\right) = 0, \tag{3.9}$$

where ϕ is continuous, diagonal, and monotonic in each component. The tridiagonal matrix A has elements

$$A_{j,j-1} = -\frac{2\xi^2}{h_j^{n+1}\left(h_{j+1}^{n+1} + h_j^{n+1}\right)}, \quad A_{j,j+1} = -\frac{2\xi^2}{h_{j+1}^{n+1}\left(h_{j+1}^{n+1} + h_j^{n+1}\right)},$$
$$A_{j,j} = \frac{\alpha\xi^2}{\Delta t^{n+1}} + \frac{2\xi^2}{h_j^{n+1}\left(h_{j+1}^{n+1}h_j^{n+1}\right)} - \frac{1}{2a}.$$

Clearly, the off-diagonal elements are always negative and the diagonal elements are positive if

$$\Delta t^{n+1} < \min_j \left(\frac{2\alpha\varepsilon^2 h_{j+1}^{n+1} h_j^{n+1}}{h_{j+1}^{n+1}h_j^{n+1} - 4\varepsilon^2} \right). \tag{3.10}$$

Hence, if (3.10) is satisfied then A is an irreducibly diagonal dominant M-matrix and hence A^{-1} exists. The existence and uniqueness of $\boldsymbol{p}_\Delta^{n+1}$ then follows from Theorem 13.1.3 of Ref. [27]. In practice, we use Newton's method to solve (3.9). Thereafter, we find $\boldsymbol{u}_\Delta^{n+1}$ by solving (3.7), which is a linear system of the form

$$C\boldsymbol{u}_\Delta^{n+1} = \boldsymbol{b}_\Delta^{n+1},$$

where $\boldsymbol{b}_\Delta^{n+1}$ is a known vector and C is an irreducibly diagonal dominant M-matrix. A unique solution is obtained since C^{-1} exists.

3.2. *Choice of Monitor Function*

The time-dependent coordinate transformation is assumed to satisfy the equidistribution principle

$$\int_0^{x(\eta,t)} M(s,t)\, ds = \eta\theta(t), \tag{3.11}$$

where

$$\theta(t) = \int_0^1 M(s,t)\, ds. \tag{3.12}$$

The monitor function M should be related to the local difficulty in solving (3.5) and (3.6). This is clearly where the phase variable changes rapidly in the interfacial region. Some guidance on the choice of an appropriate monitor function can be obtained from an asymptotic analysis of the phase field at the interface. Following Caginalp [8], we consider the phase equation (2.5a) with the free energy density given by (2.3) in the limit ξ and $a \to 0$ and α is fixed. If we let $\varepsilon^2 = \xi^2 a$ then Eq. (2.5a) can then be written as

$$\alpha\varepsilon^2 p_t = \varepsilon^2 p_{xx} + \frac{1}{2}(p - p^3) + 2au. \tag{3.13}$$

If we seek a travelling wave solution of (3.13) of the form $p = w(x/\varepsilon - vt) = w(z)$ then

$$-v\alpha\varepsilon^2 w_z = w_{zz} + \frac{1}{2}(w - w^3) + 2au.$$

If we assume that w has an asymptotic expansion $w = w^0 + \varepsilon w^1 + \cdots$, then equating zeroth-order terms and letting $a \to 0$ we find that

$$w^0_{zz} + \frac{1}{2}(w^0 - (w^0)^3) = 0. \tag{3.14}$$

The solution of (3.14) subject to the boundary conditions $w^0 \to \pm 1$ as $z \to \pm\infty$ is $w^0(z) = \tanh(z/2)$. Hence, $p(x, t)$ has an inner expansion, the zeroth-order term of which is

$$p_{\text{in}} = \tanh\left(\frac{x - s(t)}{2\varepsilon}\right), \tag{3.15}$$

where $s(t)$ denotes the position of the interface. If x_* denotes an estimate of the front position at any given time, then ideally we would like to choose a monitor function that is tailored to the profile

$$p(x) = \tanh\left(\frac{x - x_*}{2\varepsilon}\right). \tag{3.16}$$

The role of mesh equidistribution is to ensure that a nonsmooth function in Ω_{p} is mapped onto a much smoother function in Ω_{c}. For example. the steep function (3.16) can be mapped onto the straight line

$$p(\eta) = \tanh\left(-\frac{x_*}{2\varepsilon}\right) + \eta\left[\tanh\left(-\frac{(1 - x_*)}{2\varepsilon}\right) - \tanh\left(-\frac{x_*}{2\varepsilon}\right)\right]$$

by equidistributing the monitor function

$$M(x) = \operatorname{sech}^2\left(\frac{x - x_*}{2\varepsilon}\right). \tag{3.17}$$

To determine if the nonuniform mesh obtained using (3.17) is appropriate we consider the convergence of the error between $p(x)$ and its piecewise-linear interpolant $\hat{p}(x)$. A similar approximation problem is considered in [3], where it is shown that

$$\|e\|_\infty \equiv \max_{x\in(0,1)} |p(x) - \hat{p}(x)| \le CN^{-1},$$

where C is independent of ε. So while the interpolation error is uniformly convergent the

rate is suboptimal. In [3] it is also shown that second-order convergence can be obtained using the monitor function

$$M(x) = \operatorname{sech}\left(\frac{x - x_*}{2\varepsilon}\right). \tag{3.18}$$

Unfortunately, this monitor function clusters all of the mesh points within the interfacial region. As the same mesh is used to solve the heat equation it is clear that this distribution of mesh points is unsatisfactory. To ensure that mesh points are available away from the interface region we consider adding a positive floor onto the monitor function. This idea is commonly used with moving mesh techniques although the floor is often chosen on an ad hoc basis [30]. A more sensible approach is to choose the floor so that a constant proportion of the mesh points is placed external to the interfacial region and that this proportion is independent of ε. To achieve this we use the monitor function

$$M(x) = \gamma\beta + \operatorname{sech}\left(\frac{x - x_*}{2\varepsilon}\right), \tag{3.19}$$

where

$$\beta = \int_0^1 \operatorname{sech}\left(\frac{x - x_*}{2\varepsilon}\right) dx, \quad \gamma > 0. \tag{3.20}$$

An analogous approach has been used to construct suitable monitor functions for singularly perturbed boundary value problems [1, 2]. If we substitute (3.19) into (3.11) and carry the integration out exactly then the mesh points satisfy the equations

$$\gamma\beta x_j + 2\varepsilon[\sin^{-1}(\tanh((x_j - x_*)/2\varepsilon)) - \sin^{-1}(\tanh(-x_*/2\varepsilon))] = \frac{j\beta(1+\gamma)}{N}, \tag{3.21}$$

for $j = 1, \ldots, N-1$. The mesh is obtained by solving these equations using Newton's method. The parameter γ allows some flexibility in the proportion of mesh points that are placed within the interface region. For example, when x_j is outside the layer then an element of lengths $dx \subset \Omega_{\mathrm{p}}$ is related to an element $d\eta \subset \Omega_{\mathrm{c}}$ by

$$dx \approx \frac{(1+\gamma)}{\gamma}\, d\eta.$$

This shows that we have approximately $\gamma N/(1+\gamma)$ points outside the layer and $N/(1+\gamma)$ points inside the layer. For all the numerical experiments carried out in Section 5 we have set $\gamma = 1$, which allows the interface region to be well resolved while maintaining sufficient grid resolution away from the layer region.

Before we finish this section it is worth commenting on other possible monitor functions. A popular choice is the scaled solution arc length

$$M(x) = \sqrt{1 + \alpha p_x^2}, \tag{3.22}$$

where $\alpha > 0$ is a user-chosen parameter. This monitor functions forms the basis of the moving mesh method used by McCarthy [26]. One drawback of this monitor function is that it is not analytically integrable and hence the equidistrbution principle (3.11) has to

be approximated using quadrature. A more important deficiency is that the error in the piecewise-linear interpolation of (3.16) converges suboptimally on the grid obtained by equidistribution of (3.22). Numerical experiments and analysis confirming this behaviour are given in [3].

4. THE COMPLETE ALGORITHM

Each time step of the adaptive algorithm requires the solution of (3.7), (3.8), and (3.21). In theory, one could simultaneously solve this large set of differential algebraic equations. An alternative is to decouple the calculation of the mesh from the solution of the semi-discretised phase-field equations. The main advantage of this approach is the reduction in size of the algebraic systems that arise at each time step. This is the main reason why recent moving mesh methods for multidimensional problems use some form of decoupling [4, 12, 22]. An additional advantage is that decoupling allows flexibility in the choice of tolerances when determining the grid and the physical solution. As the grid is of secondary importance it is often possible to use a less strict tolerance on the convergence of the mesh. To take a time step from t^n to t^{n+1} we use the following algorithm, which is similar to that used in Mackenzie and Robertson [25]. The numerical approximation of the interface at t^n will be denoted by x_*^n.

1. Perform the simple prediction

$$x_{(*,0)}^{n+1} = x_*^n + \Delta t^{n+1}\left(\frac{x_*^n - x_*^{n-1}}{\Delta t^n}\right). \tag{4.1}$$

Set $s = 0$.

2. Let $x_* = x_{(*,s)}^{n+1}$ and solve (3.21) to give $\Delta_{N,s}^{n+1}$.

3. Solve (3.7) and (3.8) for $u_{\Delta,s}^{n+1}$ and $p_{\Delta,s}^{n+1}$. Determine $x_* = x_{(*,s+1)}^{n+1}$ using linear interpolation for $p(x_*) = 0$.

4. If $|x_{(*,s+1)}^{n+1} - x_{(*,s)}^{n+1}| < Tol_{\text{grid}}$ then $u_\Delta^{n+1} = u_{\Delta,s}^{n+1}$, $p_\Delta^{n+1} = p_{\Delta,s}^{n+1}$, $\Delta_N^{n+1} = \Delta_{N,s}^{n+1}$, and $x_*^{n+1} = x_{(*,s+1)}$. Otherwise $s = s + 1$ and go to 2.

In all the calculations presented in the following section we set $Tol_{\text{grid}} = \varepsilon/50$. The simple initial extrapolation step is extremely useful for speeding up convergence. By only extrapolating the estimate of x_* we ensure that we have a nonoverlapping grid.

5. NUMERICAL RESULTS

5.1. *A Classical Stefan Problem*

The first case we consider is a classical freezing problem in a semi-infinite plane. This allows us to compare the results using the phase-field model to the similarity solution of the classical Stefan model. Theoretically, the solution of the PF model has been shown to approach that of the Stefan model as $a, \xi \to 0$, $\sigma \to 0$, and α is fixed [8]. This example also allows us to compare the performance of our moving mesh method with fixed mesh results of Caginalp and Socolovsky [10] and the adaptive moving mesh algorithm of Blom and Zegeling [6] used by McCarthy [26].

Neumann's solution of the classical Stefan problem takes the form

$$u^{(s)}(x,t) = \begin{cases} C_1 \frac{[\operatorname{erf}(\beta/2) - \operatorname{erf}(x/(2\sqrt{t+t_0}))]}{\operatorname{erf}(\beta/2)}, & x \le s(t), \\ C_2 \frac{[\operatorname{erf}(\beta/2) - \operatorname{erf}(x/(2\sqrt{t+t_0}))]}{1-\operatorname{erf}(\beta/2)}, & x > s(t), \end{cases} \tag{5.1}$$

where t_0 is the starting time and C_1 and C_2 are constants. The position of the interface $s(t)$ is given by

$$s(t) = \beta\sqrt{t+t_0},$$

where β is the solution of

$$\frac{2}{\sqrt{\pi}} e^{-\beta^2/4}[C_2/(1-\operatorname{erf}(\beta/2)) - C_1/\operatorname{erf}(\beta/2)] - \beta = 0.$$

For computational purposes we let $0 \le x \le 1$ and choose $t_0 = 0.15$, $C_1 = -0.085$, $C_2 = -0.015$, which gives a value of $\beta = 0.396618$.

The PF calculations are performed with the values $L = K = 1$. The boundary and initial conditions for the temperature are

$$u(0,t) = C_1, \quad u(1,t) = u^{(s)}(1,t), \quad \text{and} \quad u(x,t_0) = u^{(s)}(x,t_0).$$

Remembering that the Caginalp potential $f(p,u)$ has a local minimum close to $p = -1$ and $p = 1$, we see that the boundary conditions for the phase field are

$$p(0,t) = \min_p f(p, C_1), \quad \text{closest to } -1,$$

and

$$p(1,t) = \min_p f\big(p, u^{(s)}(1,t)\big), \quad \text{closest to } 1.$$

To allow the computational mesh to be clustered around the phase front at time t_0 we use a smoothed initial value of the phase field. For this purpose we set

$$p(x,t_0) = \begin{cases} p(0,t_0)\tanh\big(\frac{s(t_0)-x}{2\varepsilon}\big), & x \le s(t_0), \\ p(1,t_0)\tanh\big(\frac{x-s(t_0)}{2\varepsilon}\big), & x \ge s(t_0). \end{cases} \tag{5.2}$$

We first consider the results with the parameters $a = 0.0625$, $\xi = 0.002$, and $\alpha = 1$. These values lead to an interface thickness $\varepsilon = 0.0005$ and a surface tension $\sigma = 0.00533$. This case corresponds to experiment 5 of Caginalp and Socolovsky [10] and is a stiff test for a fixed grid method. In fact it is not possible to compute an accurate solution up to $t = 1$ using $N = 1000$ uniform mesh intervals. However, Fig. 2 shows the computed interface position and mesh trajectories using the moving mesh method with $N = 50$ and $\Delta t = 5 \times 10^{-3}$. We can see that the mesh points move smoothly and the predicted interface position is very accurate. Figure 3 shows the temperature profiles at $t = 0$, 0.2, and 1. To plotting accuracy the moving grid results are indistinguishable from the Neumann solution. The temperature history at the point $x = 0.18$ is also shown in Fig. 3. As pointed out by Fabbri and Voller

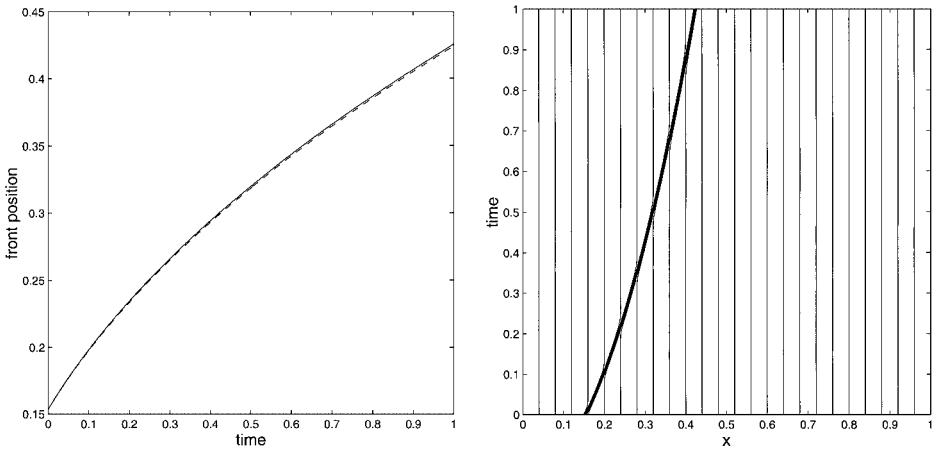

FIG. 2. (Left) Interface positions (— Neumann, - - - moving mesh) and (right) mesh trajectories for phase-field approximation of a classical Stefan problem.

[18], this type of plot is severe check of the numerical method and we can see clearly that the moving mesh method performs excellently. The ability of the moving mesh method to adapt to different interface thicknesses is shown in Fig. 4, where we have plotted the phase and temperature fields at $t = 1$. Note that the grids have an equal number of points within the interface independently of ε and that the interface position is relatively insensitive to ε. These results are an improvement on those computed by McCarthy [26]. This can mainly be attributed to an appropriate choice of monitor function and a suitable initial mesh. Table I shows the results obtained for the parameter values considered in [10]. The accuracy using the moving mesh method is comparable with those presented in [10], although we have only used $N = 50$ points throughout. The remaining error in the front position is mainly due to the small but nonzero value of σ which we have used in the computations. The fact that the normalised CPU time does not increase dramatically as $\varepsilon \to 0$ demonstrates the

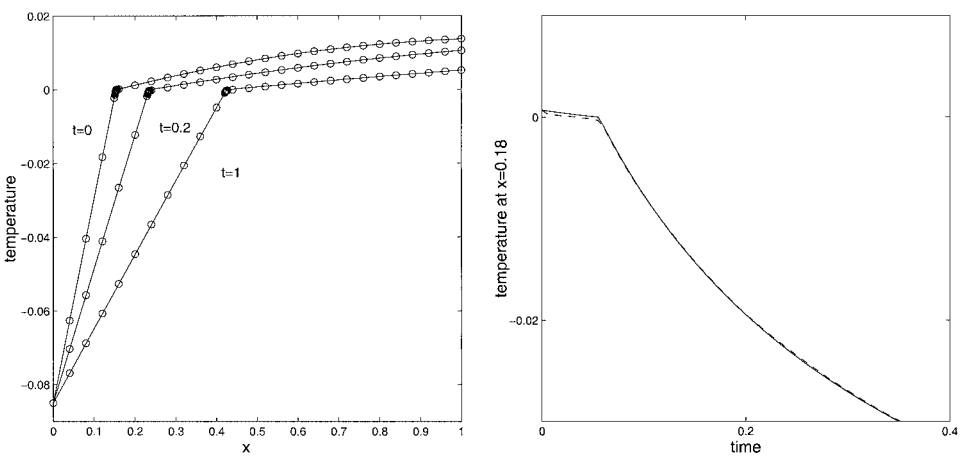

FIG. 3. (Left) Temperature profiles (— Neumann, ○ moving mesh) and (right) the temperature history at $x = 0.18$ (— Neumann, - - - moving mesh) for phase-field approximation of a classical Stefan problem.

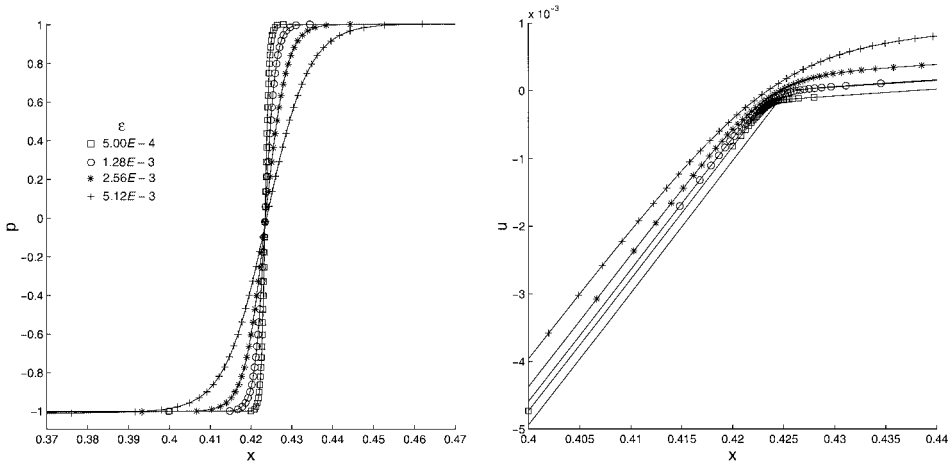

FIG. 4. (Left) Phase and (right) temperature fields at $t = 1$ for classical Stefan problem.

efficiency and robustness of the moving mesh algorithm. It should be noted that in [10] the authors report an increase in CPU time of a factor of 8.59 when ε goes from 0.00512 to 0.00128 using a uniform mesh method.

5.2. *A Modified Stefan Problem*

The sharp interface problem with nonzero values of α and σ is of considerable practical importance. Following Fabbri and Voller [18] and McCarthy [26], we consider a test case similar to the previous example. We will assume that classical Stefan solidification occurs from $t = 0$ to $t_0 = 0.1846$. At this time we assume that the interface has reached the position $x_0 = 0.14$ and has a velocity $v_0 = 0.4616$. Given values of σ and ε we can determine ξ and a for the Caginalp potential from (2.4). At t_0 we trigger the undercooling effect be specifying an initial temperature of the interface, u_0, and α is determined from the one-dimensional Gibbs–Thompson relation

$$-u_0 = -\frac{\alpha\sigma}{\Delta s} v_0. \tag{5.3}$$

The aim of this example is to check how well the solution of the PF equations satisfies (5.3), which holds for the sharp-interface modified Stefan model. Figure 5 shows the evolution of the front temperature and the front position for the two cases $u_0 = -0.01$ and

TABLE I

Differences in Interface Position between Adaptive PF Calculations Using the Caginalp Potential and the Neumann Solution of a Classical Stefan Problem: $N = 50$, $\Delta t = 5 \times 10^{-3}$, and $\sigma = 0.0053$

a	ξ	ε	$\|e_f\|_\infty$	$\|e_f\|_{t=1}$	CPU
0.64	6.4E−3	5.12E−3	2.744E−3	2.733E−3	1.00
0.32	4.5255E−3	2.56E−3	3.540E−3	3.450E−3	1.07
0.16	3.2E−3	1.28E−3	3.958E−3	3.690E−3	1.21
0.0625	2.0E−3	5.00E−4	4.019E−3	3.578E−3	2.16

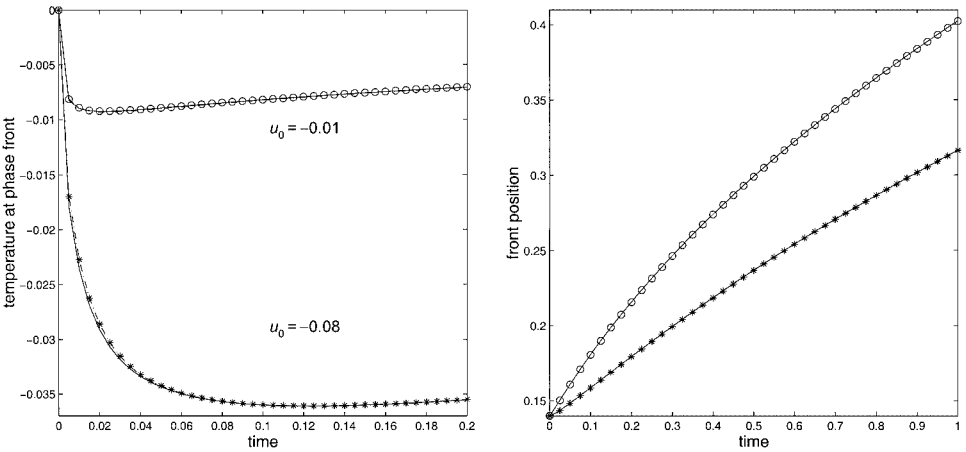

FIG. 5. (Left) Temperature and (right) front position for modified Stefan problem with $u_0 = -0.01$ and $u_0 = -0.08$. Gibbs–Thompson relation ---, fine moving mesh - - -, moving mesh $N = 50$, ○, ✻.

$u_0 = -0.08$. The results were obtained using the parameters $\xi = 0.002$, $a = 0.0625$, $N = 50$, and $\Delta t = 5 \times 10^{-3}$. For comparison we have also included solutions obtained using a fine moving mesh with $N = 250$. We have compared the computed temperature on the interface with the temperature obtained from (5.3), where the velocity of the front is approximated by numerical differentiation. We can see that the agreement is excellent for both values of u_0. The computed front positions are also well predicted in comparison with the fine moving mesh results.

5.3. *Planar Solidification*

A popular test case is to reproduce the travelling wave solution of the growth of a solid planar interface within an undercooled melt. This problem has also been considered in [7], [11], and [23]. The sharp interface equations (2.1) are solved with boundary conditions

$$u(\infty) = u_{\text{cool}}, \quad u(-\infty) = u_{\text{cool}} + 1.$$

It is easy to show that there exists a travelling wave solution which takes the form

$$u(x,t) = \begin{cases} u_{\text{cool}} + e^{-v^*(x-v^*t)/K}, & x > v^*t, \\ u_{\text{cool}} + 1, & x \le v^*t, \end{cases} \tag{5.4}$$

where the velocity

$$v^* = -\frac{\varepsilon}{6\alpha a}(u_{\text{cool}} + 1). \tag{5.5}$$

A travelling wave solution of the PF equations can be found by writing them with respect to a reference frame moving to the right with speed $v(\varepsilon)$. This gives rise to the set of equations

$$v(\varepsilon)u_\eta + \frac{v(\varepsilon)}{2}p_\eta + Ku_{\eta\eta} = 0, \tag{5.6}$$

$$\alpha\varepsilon^2 v(\varepsilon)p_\eta + \varepsilon^2 p_{\eta\eta} + \frac{1}{2}(p - p^3) + 2au = 0, \tag{5.7}$$

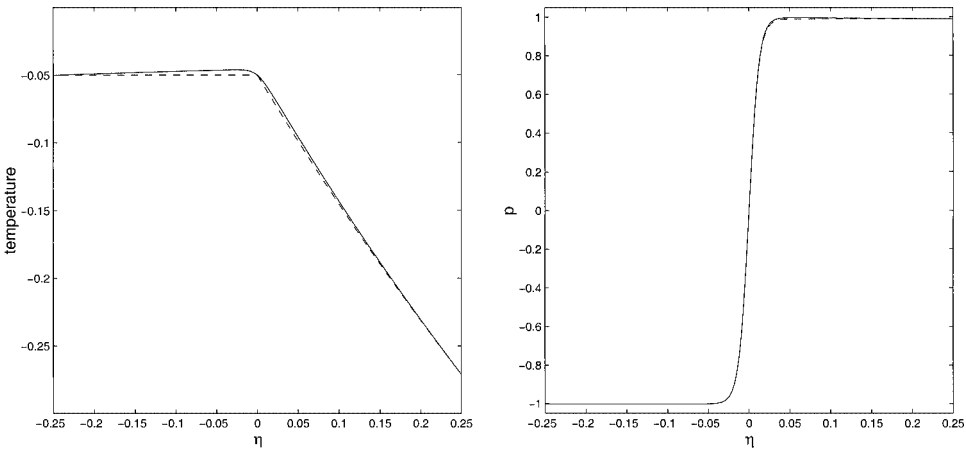

FIG. 6. Travelling wave profiles of u and p for phase-field equations with $\alpha = 1, \varepsilon = 0.00625$, and $a = 0.02083$.

where $\eta = x - v(\varepsilon)t$. We attempt to find a solution of these equations using central difference approximations of the derivatives. In addition, we fix the interface value so that $p(0) = 0$. The discretised equations are solved using Newton's method on an adapted mesh with $N = 200$ points using monitor function (3.18) with $\gamma = 1$. For numerical purposes we have truncated the computational domain so that $\eta \in [-d, d]$, where d is chosen to be much larger than the interface thickness. At the domain boundaries we apply the conditions

$$u(d) = u_{\text{cool}} + e^{-v^* d/K}, \quad u(-d) = u_{\text{cool}} + 1$$

and compatible Dirichlet conditions for $p(\pm d)$. Figure 6 shows the profiles for u and p when $u_{\text{cool}} = -1.05$, $d = 0.25$, $K = \alpha = 1$, $\varepsilon = 0.00625$, and $a = 0.02083$. With these parameters the sharp-interface problem has a travelling wave solution with $v^* = 1$. For comparison we have also included the sharp-interface solution for u, which is shown using a dotted line. We can see that we have reasonable agreement for this value of ε. Along with the computed phase profile we have also plotted the function

$$\bar{p}(\eta) = \begin{cases} p(-d)\tanh\left(\frac{\eta}{2\varepsilon}\right), & \eta \le 0, \\ p(d)\tanh\left(\frac{\eta}{2\varepsilon}\right), & \eta > 0, \end{cases}$$

which is shown using a dotted line. Clearly, there is excellent agreement between these two functions, especially in the interface region. The velocity $v(\varepsilon)$ with these parameters was found to be 1.0430, slightly faster than that for the sharp-interface problem. It has been shown in [9] that the velocity $v(\varepsilon) \to v^*$ as $\varepsilon \to 0$ and that the temperature converges uniformly to (5.4) with respect to η. An important question is how quickly $v(\varepsilon) \to v^*$. Figure 7 shows that the phase-field velocity appears to converge at a rate that is first order in ε. This rate is in agreement with the numerical simulations of Elliott and Gardiner [17].

The results from the steady calculation are then used as initial conditions for the full time-dependent problem. Figures 8a and 8b show the profiles of u and p as solid lines along with the travelling wave profiles advected along with the wave speed $v(\varepsilon)$. These results were calculated with $\Delta t = 10^{-3}$, $N = 50$, and $\gamma = 1$ and are shown at times $t = 0.02$, 0.04, 0.06, 0.08, 0.1. It can be seen that the time-dependent results follow the travelling

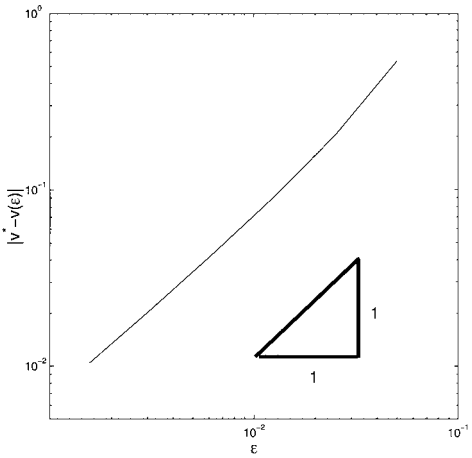

FIG. 7. Convergence of $v(\varepsilon)$ to v^* as $\varepsilon \to 0$.

wave solution extremely well. Table II compares the discrete L_2 error in the temperature at $t = 0.1$ with two sets of results from Elliott and Gardiner [17]. These were obtained using the usual quartic potential model, PF, and a model using a double-obstacle potential, PFO. We can see that for the two larger values of ε, our results are a distinct improvement over those obtained in [17], where the authors used a uniform mesh with $N = 300$ grid points and 900 time steps. No result is quoted for either technique used by Elliott and Gardiner for the smallest value of ε. It can be assumed that the authors would have found it difficult to take such a small value of ε using only $N = 300$ uniform mesh nodes since there would an insufficient number to resolve the interface region.

5.4. *The Critical Radius of Instability of Solidification*

Our final test case involves the stability of a solid sphere in equilibrium with its melt. If the sphere has κ_0 as its sum of principle curvatures, and both the solid and liquid are at a

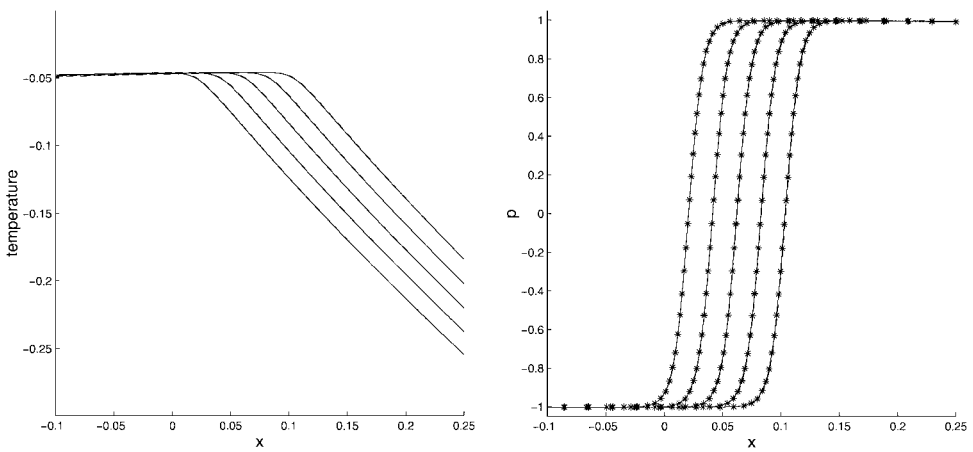

FIG. 8. (Left) Temperature and (right) phase variable profiles for planar solidification with $\varepsilon = 0.00625$ and $a = 0.02083$.

TABLE II
Discrete L_2 Error in u at $t = 0.1$ for Time-Dependent Travelling Wave Problem

ε	PF [17]	PFO [17]	Adaptive
0.02	5.23E−3	3.06E−3	2.10E−3
0.01	2.60E−3	1.33E−3	1.15E−3
0.00625	—	—	9.53E−4

constant temperature, u_0, then according to the Gibbs–Thompson relation

$$u_0 = -\sigma_0 \kappa_0 / 4. \tag{5.8}$$

Following Caginalp [10], we consider the domain $1 \le r \le 2$, with $K = 10$, $L = 0.1$, and $\alpha = 1$. The equilibrium position of the interface is chosen to be $r_0 = 1.5$, leading to an initial value for the curvature $\kappa_0 = 4/3$. The surface tension is chosen to be $\sigma_0 = 0.15$, so according to (5.8) the initial temperature $u_0 = -0.05$. The boundary conditions for the temperature are $u(1, t) = u(2, t) = u_0$. The initial condition for the phase field is given by (5.2) for various values of the initial position, s_0, of the solid sphere's surface. The equilibrium situation has been shown to be unstable in that if the initial interface $s_0 < 1.5$ then the solid sphere melts inwards, whereas if $s_0 > 1.5$ then the sphere solidifies outwards [13]. The situation when $s_0 \approx 1.5$ is therefore a very severe test of any numerical method.

Due to the spherical symmetry of the problem the governing equations can be written in terms of the radius r as

$$\alpha \xi^2 \frac{\partial p}{\partial t} = \xi^2 \left(\frac{\partial^2 p}{\partial r^2} + \frac{2}{r} \frac{\partial p}{\partial r} \right) - \frac{\partial f}{\partial p}, \tag{5.9}$$

$$\frac{\partial u}{\partial t} + \frac{L}{2} \frac{\partial p}{\partial t} = K \left(\frac{\partial^2 u}{\partial r^2} + \frac{2}{r} \frac{\partial p}{\partial r} \right). \tag{5.10}$$

The spatial discretisation of (5.9) and (5.10) is again achieved using second-order central difference operators. Figures 9 and 10 show results for various values of s_0 with

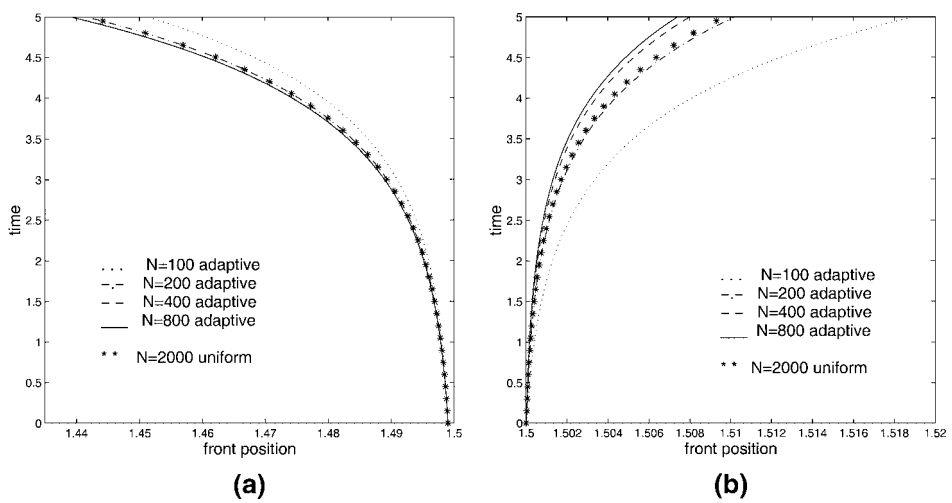

FIG. 9. Front positions for sphere solidification problem. (a) $s_0 = 1.499$; (b) $s_0 = 1.5$.

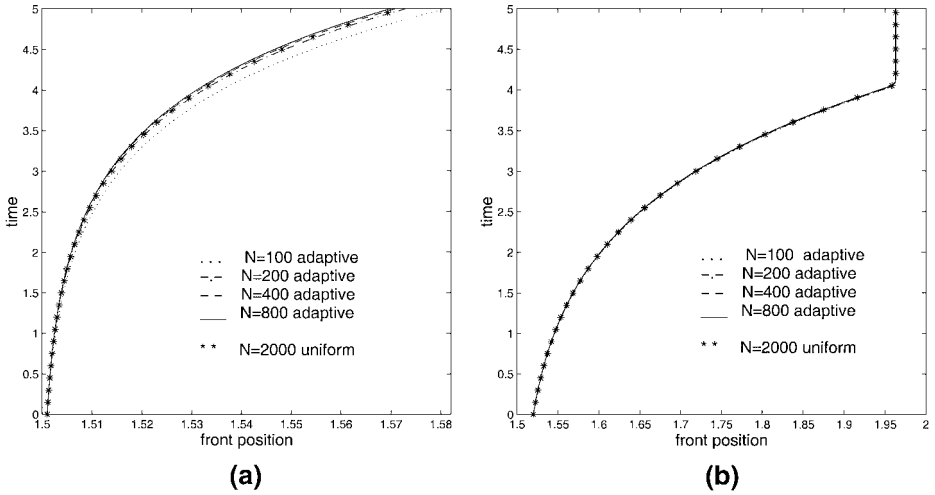

FIG. 10. Front positions for sphere solidification problem. (a) $s_0 = 1.501$; (b) $s_0 = 1.52$.

$\xi = 0.045$, $a = 0.04$, leading to an interface thickness $\varepsilon = 0.009$. For comparison, we have also computed solutions using a fine uniform mesh with $N = 2000$ and $\Delta t = 5 \times 10^{-3}$. When $s_0 = 1.499$ we find that the sphere melts inwards as predicted. The adaptive grid results show a similar behaviour using an order-of-magnitude less mesh points, resulting in a reduction in CPU time by a factor of 50. Similarly, with $s_0 = 1.5$ we find that we consistently predict that the sphere solidifies outwards. Caginalp and Socolovsky [10] predict a similar behaviour using a very fine uniform mesh. However, it is interesting to note that McCarthy [26] fails to calculate consistent results. The author concludes that moving mesh methods are not suitable for this problem due to the sensitivity of results on the temporal smoothing parameter which is part of the Blom and Zegeling algorithm. However, it is clear from our results that the combination of an appropriate initial grid and the lack of any temporal smoothing parameter improves the robustness of the predictions. Finally, Fig. 10 shows that when $s_0 > 1.5$ we always observe the sphere solidifying outwards.

6. CONCLUSIONS

In this paper we have presented a simple moving mesh algorithm for the solution of the one-dimensional phase-field equations. The method gives rise to smooth mesh trajectories and results in significant efficiency savings over uniform mesh methods. The proposed monitor function automatically clusters mesh points around the phase-change interface and scales appropriately with its thickness. We have also proved that the system of nonlinear algebraic equations arising from the discretisation on the moving mesh has a unique solution for a small enough time step.

Recent work has concentrated on the development of the ideas presented here to two-dimensional problems. These are incorporated within a moving finite element framework which we have developed for two-dimensional classical Stefan problems [4]. Progress in this area is reported in [5].

REFERENCES

1. G. Beckett and J. A. Mackenzie, Convergence analysis of finite-difference approximations on equidistributed grids to a singularly perturbed boundary value problem, *Appl. Numer. Math.* **35**, 7 (2000).
2. G. Beckett and J. A. Mackenzie, On a uniformly accurate finite difference approximation of a singularly perturbed reaction–diffusion problem using grid equidistribution, *J. Comput. Appl. Math.* **131**, 381 (2001).
3. G. Beckett, J. A. Mackenzie, A. Ramage, and D. M. Sloan, On the numerical solution of one-dimensional PDEs using adaptive methods based on equidistribution, *J. Comput. Phys.* **167**, 372 (2001).
4. G. Beckett, J. A. Mackenzie, and M. L. Robertson, A moving mesh finite element method for the solution of two-dimensional Stefan problems, *J. Comput. Phys.* **168**, 500 (2001).
5. G. Beckett, J. A. Mackenzie, and M. L. Robertson, *An r-Adaptive Finite Element Method for the Solution of the Two-Dimensional Phase-Field Equations*, Technical Report 32 (Strathclyde University, Mathematics Department, 2001), submitted for publication.
6. J. G. Blom and P. A. Zegeling, A moving-grid interface for systems of one-dimensional time dependent partial differential equations, *ACM Trans. Math. Software* **20**, 194 (1994).
7. R. J. Braun, G. B. McFaddenn, and S. R. Coriell, Morphological instability in phase-field models of solidification, *Phys. Rev. E* **49**, 4336 (1994).
8. G. Caginalp, Stefan and Hele–Shaw type models as asymptotic limits of the phase-field equations, *Phys. Rev. A* **39**, 5887 (1989).
9. G. Caginalp and Y. Nishiura, The existence of travelling waves for phase field equations and convergence to sharp interface models in the singular limit, *Q. Appl. Math.* **49**, 147 (1991).
10. G. Caginalp and E. A. Socolovsky, Computation of sharp phase boundaries by spreading: The planar and spherically symmetric cases, *J. Comput. Phys.* **95**, 85 (1991).
11. G. Caginalp and E. A. Socolovsky, Phase field computations of single-needle crystals, crystal growth, and motion by mean curvature, *SIAM J. Sci. Comput.* **15**, 106 (1994).
12. W. Cao, W. Huang, and R. D. Russell, An r-adaptive finite element method based upon moving mesh PDEs, *J. Comput. Phys.* **149**, 221 (1999).
13. B. Chalmers, *Principles of Solidification* (Krieger, New York, 1977).
14. J. Crank, *Free and Moving Boundary Value Problems* (Oxford Science, Oxford, UK, 1984).
15. C. de Boor, Good approximation by splines with variables knots II, in *Lecture Notes in Mathematics* (Springer-Verlag, Berlin/New York, 1974). Vol. 363, pp. 12–20.
16. E. A. Dorfi and L. O'c. Drury, Simple adaptive grids for 1-D initial value problems, *J. Comput. Phys.* **69**, 175 (1987).
17. C. M. Elliott and A. R. Gardiner, One dimensional phase field computations, *Pitman Res. Notes Math.* **23**, 56 (1993).
18. M. Fabbri and V. R. Voller, The phase-field method in the sharp-interface limit: A comparison between model potentials, *J. Comput. Phys.* **130**, 256 (1997).
19. K. Farrell and L. Drury, An explicit, adaptive grid algorithm for one-dimensional initial value problems, *Appl. Numer. Math.* **26**, 3 (1997).
20. W. Huang, Y. Ren, and R. D. Russel, Moving mesh PDEs based on the equidistribution principle, *SIAM J. Numer. Anal.* **31**, 709 (1994).
21. W. Huang and R. D. Russell, Analysis of moving mesh partial differential equations with spatial smoothing, *SIAM J. Numer. Anal.* **34**, 1106 (1997).
22. W. Huang and R. D. Russell, A high dimensional moving mesh strategy, *Appl. Numer. Math.* **26**, 63 (1997).
23. A. Karma and W.-J. Rappel, Quantitative phase-field modeling of dendritic growth in two and three dimensions, *Phys. Rev. E* **57**, 4323 (1998).
24. R. Kobayashi, Modeling and numerical simulations of dendritic growth, *Physica D* **63**, 410 (1993).
25. J. A. Mackenzie and M. L. Robertson, The numerical solution of one-dimensional phase change problems using an adaptive moving mesh method, *J. Comput. Phys.* **161**, 537 (2000).

26. J. F. McCarthy, One-dimensional phase field models with adaptive grids, *Trans. ASME* **120**, 956 (1998).
27. J. M. Ortega and W. C. Rheinboldt, *Iterative Solution of Nonlinear Equations in Several Variables* (Academic Press, San Diego 1970).
28. O. Penrose and P. C. Fife, On the relation between the standard phase-field model and a thermodynamically consistent phase-field model, *Physica D* **69**, 107 (1993).
29. N. Provatas, N. Goldenfeld, and J. Dantzig, Efficient computation of dendritic microstructures using adaptive mesh refinement, *Phys. Rev. Lett.* **80**(15), 3308 (1998).
30. J. D. Pryce, On the convergence of iterated remeshing, *IMA J. Numer. Anal.* **9**, 315 (1989).
31. A. Schmidt, Computation of three dimensional dendrites with finite elements, *J. Comput. Phys.* **125**, 293 (1996).
32. S.-L. Wang, R. F. Sekerka, A. A. Wheeler, B. T. Murray, S. R. Coriell, R. J. Braun, and G. B. McFadden, Thermodynamically-consistent phase field-models for solidification, *Physica D* **69**, 189 (1993).
33. A. A. Wheeler, B. T. Murray, and R. J. Schaefer, Computation of dendrites using a phase field model, *Physica D* **66**, 243 (1993).